
SYNTHESIS AND PROPERTIES OF INORGANIC COMPOUNDS

Evolution of Composition and Fractal Structure of Hydrous Zirconia Xerogels during Thermal Annealing

V. K. Ivanov^a, G. P. Kopitsa^b, A. E. Baranchikov^a, S. V. Grigor'ev^b, and V. M. Haramus^c

^a Kurnakov Institute of General and Inorganic Chemistry, Russian Academy of Sciences,
Leninskii pr. 31, Moscow, 119991 Russia

^b Institute of Nuclear Physics, Russian Academy of Sciences, Gatchina, Leningrad oblast, 188300 Russia

^c GKSS Research Centre, Geesthacht, Germany

Received June 23, 2009

Abstract—The mesostructure of amorphous hydrous zirconia xerogels and the products of their heat treatment was studied for the first time using powder X-ray diffraction and small-angle neutron scattering (SANS). The samples prepared at low and high pH values have fundamentally different phase compositions and structures. The high-temperature annealing of hydrous zirconia xerogels is useful for manufacturing materials with controlled surface fractal dimensions.

DOI: 10.1134/S0036023610020038

Fractal geometry has recently come into use in various fields of inorganic chemistry and materials science for the description of complex systems that have scaling symmetry, that is, a self-similarity of components within a certain range of linear sizes. Fractal dimension D , a quantitative characteristic of such systems, is directly related to their structure-sensitive properties, such as adsorption capacity, catalytic activity, and reactivity [1]. Importantly, in some cases fractal geometry principles offer the only means for quantifying the functional properties of compounds and materials.

An experimental quantification of the influence of fractal dimension on the structure-sensitive properties of physicochemical systems requires the existence of processes for preparing materials with controlled surface fractal dimensions where self-similarity exists over a wide range of sizes. The inspection of the related literature shows that, although seeming diversified, most of the existing processes for preparing fractal structures are based on few models and experimental procedures that have appeared as early as at the initial stages of investigation of fractal manifestations in physicochemical systems [2]. Methods employing various particle aggregation modes in liquid and gas phases have been mostly developed. However, these methods are frequently unsuitable for preparing solid-phase materials or do not produce materials with desired fractal dimensions.

Earlier [3, 4], we demonstrated that high-temperature annealing may be regarded as an efficient means for altering the fractal properties of the material. In this work, we highlight the trends of the alteration of

the chemical and phase composition and surface fractal dimension during the annealing of hydrous zirconia xerogels.

EXPERIMENTAL

Hydrous ZrO_2 xerogels were prepared as follows: to an aqueous solution of zirconyl nitrate $ZrO(NO_3)_2$ (0.25 mol/L), aqueous ammonia (2.7 mol/L) was added with stirring until the solution acquired a set pH value (3, 6, or 9). The precipitates were centrifuged from the mother solution, washed with distilled water, and dried in air at 60°C for 6 h. Then, the xerogels were annealed for 5 h at 270–600°C. In this way, for each precipitation pH value five samples were prepared using differing annealing temperatures ($T_a = 60, 270, 380, 500$, and 600°C).

Thermogravimetric analysis (TGA) and differential thermal analysis (DTA) were performed on a Pyris Diamond (Perkin-Elmer) thermal analyzer in the range 20–1000°C in air. The heating rate was 10 K/min.

Powder X-ray diffraction analysis was carried out on a Rigaku D/MAX 2500 diffractometer ($CuK\alpha$ radiation). Diffraction peaks were identified with reference to the JCPDS database. The diffraction patterns were recorded in the 5°–60° (2θ) range in 0.02° steps. Coherent scattering lengths for tetragonal and monoclinic ZrO_2 were determined from the Debye–Scherer relationship

$$D_{CSL} = 0.9\lambda / \beta \cos\theta, \quad (1)$$

where λ is the X-ray wavelength and β is the width-at-half-height of the diffraction peak.

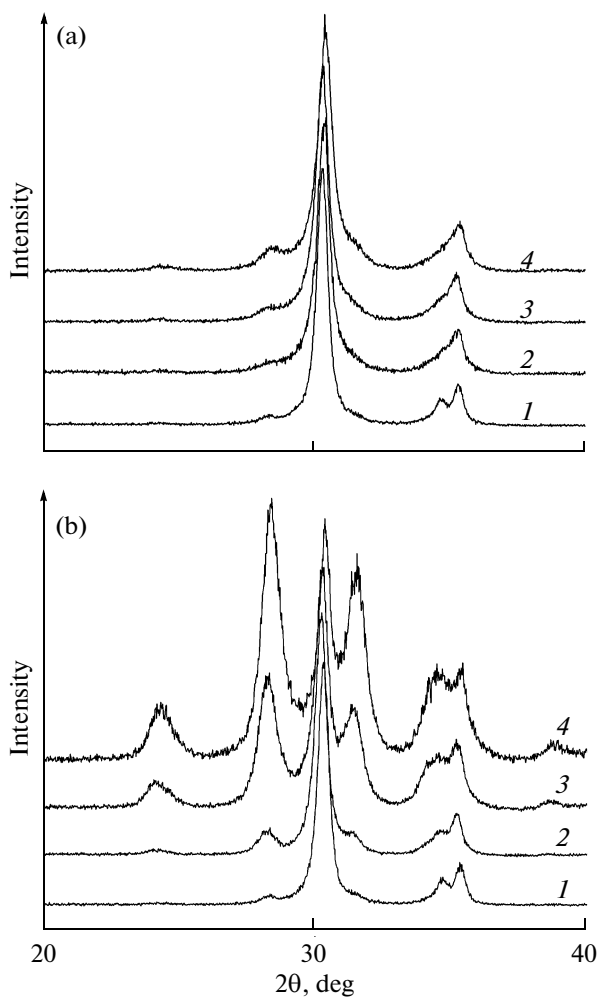


Fig. 1. Fragments of X-ray diffraction patterns for samples prepared by annealing $\text{ZrO}_2 \cdot x\text{H}_2\text{O}$ xerogels at (a) 500 and (b) 600°C: (1–4) annealing products of the xerogel prepared at pH of 3, 6, 7.5, and 9, respectively.

The contents of monoclinic (m-ZrO_2) and tetragonal (t-ZrO_2) phases in samples (x_m and x_t , respectively) were derived from X-ray diffraction data using the relationships found in [5]:

$$x = \frac{I_m(\bar{1}11) + I_m(111)}{I_m(\bar{1}11) + I_m(111) + I_t(111)}, \quad (2)$$

$$v_m = \frac{1.311x}{1 + 0.311x}, \quad (3)$$

$$v_t = 1 - v_m, \quad (4)$$

Here, $I_m(\bar{1}11)$ and $I_m(111)$ are the integrated intensities of the $(\bar{1}11)$ and (111) m-ZrO_2 peaks, respectively; $I_t(111)$ is the integrated intensity of the (111) peak of t-ZrO_2 ; and v_m and v_t are the volume fractions of monoclinic and tetragonal zirconia in the test sample.

Small-angle neutron scattering (SANS) was measured on a SANS-1 setup (FRG1 reactor, GKSS Research Centre, Geesthacht, Germany) [6] operating in a geometry close to point geometry. The neutron wavelength $\lambda = 8.19 \text{ \AA}$; $\Delta\lambda/\lambda = 10\%$. The measurements were carried out at four sample-detector distances ($SD = 0.7, 1.8, 4.5$, and 9 m), which allowed neutron scattering intensities to be measured in the momentum transfer range of $4.5 \times 10^{-3} < q < 2.5 \times 10^{-1} \text{ \AA}^{-1}$. Scattered neutrons were detected by a ${}^3\text{He}$ position-sensitive area detector.

$\text{ZrO}_2 \cdot x\text{H}_2\text{O}$ samples were placed to 1-mm quartz glass cells. As-recorded spectra for each q range were corrected for the scattering from the setup hardware, cell, and ambience using a standard procedure [7]. The thus-obtained two-dimensional isotropic spectra were azimuthally averaged and reduced to absolute magnitudes via scaling to the incoherent scattering cross section of 1 mm of water H_2O with account for the detector efficiency [7] and bulk density ρ_b for each sample. All measurements were carried out at room temperature.

The SANS intensity $I_s(q)$ was determined in this work as

$$I_s(q) = I(q) - TI_0(q), \quad (5)$$

Here, $I(q)$ and $I_0(q)$ are q distributions for scattered neutrons behind the sample and for the beam without test sample, respectively; and $T = I/I_0 = e^{(-\Sigma L)}$ is the transmission coefficient for neutrons behind the sample, where $\Sigma = \sigma_s + \sigma_a$ is the integrated cross section, including nuclear scattering σ_s and absorption σ_a ; and L is the sample thickness.

The setup resolution function was fitted to a Gaussian and calculated separately for each SD distance using a routine procedure [8].

RESULTS AND DISCUSSION

Thermal analysis shows that all tested $\text{ZrO}_2 \cdot x\text{H}_2\text{O}$ xerogels decompose by a complex scenario. At temperatures below 220–240°C, the weight loss is exclusively due to the elimination of sorbed and chemically bound water. A subsequent rise in temperature leads to a noticeable increase in weight loss rate, which may arise from the concurrent dehydration of the xerogels and elimination of residual nitrato groups.

Powder X-ray diffraction shows that all as-synthesized xerogels, as well as the samples annealed at 270°C for 5 h, are X-ray amorphous; broad maxima at ~30° and ~50°–60° 2θ appear in the relevant diffraction patterns. Where the annealing temperature rises to 380°C, the thermolysis product of the xerogels in all cases is tetragonal zirconia (t-ZrO_2). Lastly, the composition of the annealing products at 500 and 600°C considerably depends on xerogel preparation parame-

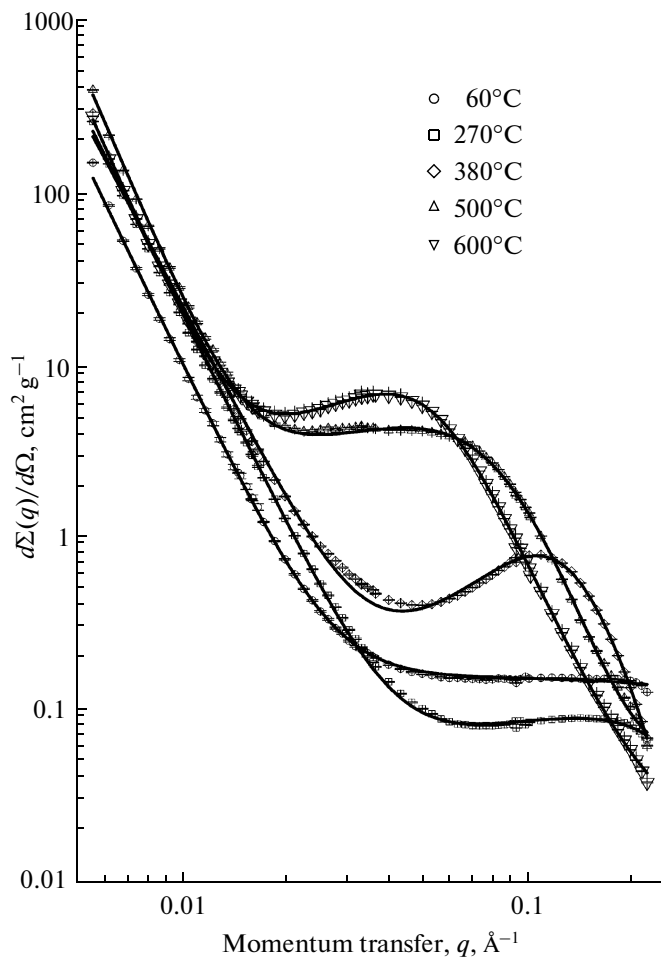


Fig. 2. Differential SANS cross section $d\Sigma(q)/d\Omega$ for the xerogel prepared at pH 3 and its annealing products. Here and in Figs. 3 and 4, solid lines are best-fit curves obtained using Eqs. (6) and (7).

ters. In particular, as pH at which $\text{ZrO}_2 \cdot x\text{H}_2\text{O}$ gels were precipitated increases, the percentage of monoclinic ZrO_2 (m-ZrO_2) in the annealing products increases systematically, whereas the t-ZrO_2 percentage decreases (Fig. 1). This effect is probably caused by the stabilization of tetragonal ZrO_2 by residual nitroso groups [9]. Noteworthy, an increase in precipitation pH also entails a decrease in particle sizes of the t-ZrO_2 and m-ZrO_2 phases that are formed during the thermal degradation of xerogels.

Figures 2–4 display the $d\Sigma(q)/d\Omega$ scattering curves for amorphous xerogel samples based on hydrous ZrO_2 (precipitated at pH of 3, 6, and 9, respectively) after annealing at various temperatures T_a . For all xerogels studied, regardless of precipitation pH, the scattering cross section $d\Sigma(q)/d\Omega$ increases with rising T_a virtually over the entire range of the momentum transfers studied (q). Noteworthy, this increase is evidently non-uniform and depends on T_a .

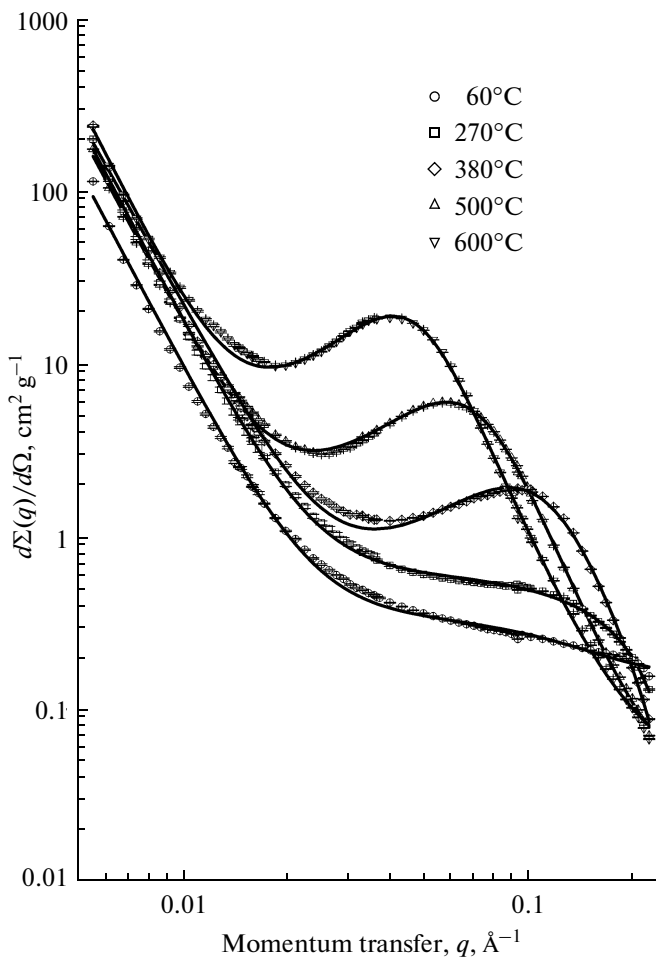


Fig. 3. Differential SANS cross section $d\Sigma(q)/d\Omega$ for the xerogel prepared at pH 6 and its annealing products.

A common feature of all xerogel samples and their annealing products is the existence of two q ranges on the scattering curves where the behavior of the small-angle cross section $d\Sigma(q)/d\Omega$ is dramatically different. In the range where $q < q_c$ (q_c is the transition point from one scattering mode to another), for all samples $d\Sigma(q)/d\Omega$ obeys the exponential law q^{-n} .

The exponent n values found from the slopes of linear segments of the experimental log–log $d\Sigma(q)/d\Omega$ curves for the xerogels prepared at pH of 6 and 9 and their annealing products fall in the range from 3.38 to 3.99, these values increasing in response to increasing gel precipitation pH and annealing temperature. When $3 < n \leq 4$, this means that for all test samples there is scattering from fractal surfaces with dimensions of $2 \leq D_s = 6 - n < 3$. This result completely matches the previous observation [10] of scattering from a porous structure with a fractal interface in amorphous hydrous zirconia xerogels precipitated

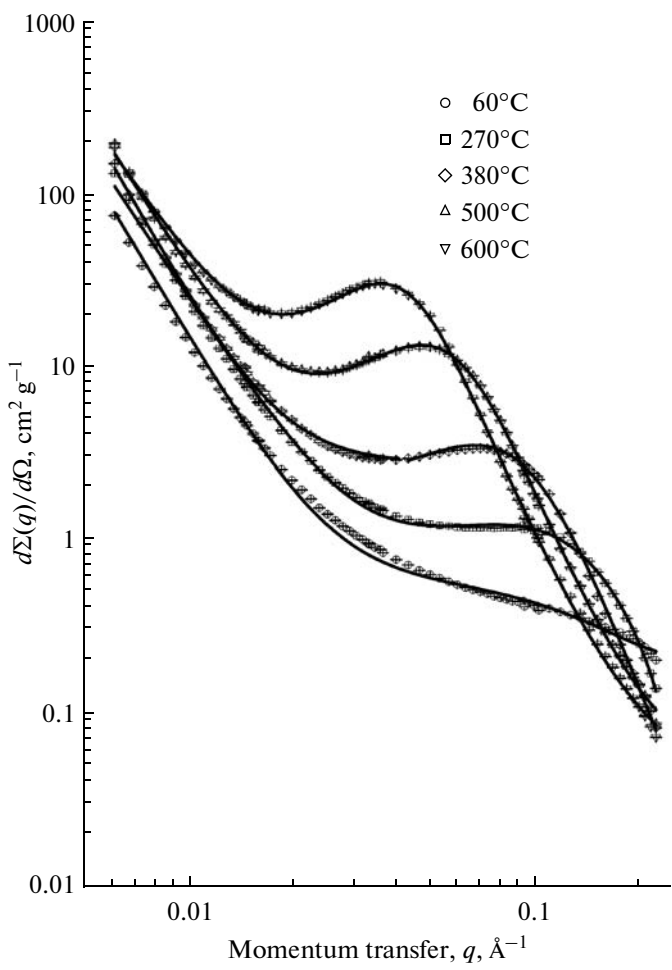


Fig. 4. Differential SANS cross section $d\Sigma(q)/d\Omega$ for the xerogel prepared at pH 9 and its annealing products.

from aqueous zirconyl nitrate solutions with pH above 6. Therefore, in further analysis of scattering for $q < q_c$, we used the two-phase (solid–pore) model of a porous structure with a fractal interface [10].

In the range where $q > q_c$, the behavior of small-angle scattering cross section $d\Sigma(q)/d\Omega$ is an explicit function of annealing temperature. At $T_a \leq 270^\circ\text{C}$, for example, the scattering curves feature a so-called shoulder indicating the existence of small monodisperse inhomogeneities with an effective gyration radius of $r_g = (3/5)^{1/2}r_0$ (where r_0 is the maximal size of monodisperse inhomogeneities). A rise in annealing temperature to $\geq 380^\circ\text{C}$ or higher transforms this shoulder to a broad maximum, in our opinion, as a result of the appearance of a short-range order in the system.

Thus, the observed scattering pattern signifies the existence of two types of scattering inhomogeneities in the test samples, these inhomogeneities strongly differing in characteristic scales. The as-precipitated

xerogels and the products of their heat treatment at 270°C consist of aggregates with a well developed surface built of small monodisperse monomeric particles. A further elevation of the annealing temperature to 380°C or higher brings about the appearance of a crystalline phase whose particle sizes increase with T_a . These results match the above-described powder X-ray powder diffraction data. Comparing SANS data for the as-precipitated xerogels also shows that the incoherent scattering background for $q > 0.03 \text{ \AA}^{-1}$ increases with precipitation pH indicating the increased contents of sorbed and chemically bound water of the xerogels.

Scattering from amorphous samples that has been annealed at or below $\leq 270^\circ\text{C}$ was analyzed as [10, 11]

$$\frac{d\Sigma(q)}{d\Omega} = \frac{A_1(D_S)}{q^n} + A_2 \exp\left(-\frac{q^2 r_g^2}{3}\right) + I_{\text{inc}}, \quad (6)$$

where $A_1(D_S)$ and A_2 are free parameters, the former being a function of the fractal dimension of the system [12] and the latter directly proportional to the product of the number of monodisperse inhomogeneities in the scattering volume and the density of neutron scattering amplitude ρ on these inhomogeneities [13]. The parameter I_{inc} is a q -independent constant caused by incoherent scattering on hydrogen atoms contained in the sample in the form of chemically bound water.

In analyzing $d\Sigma(q)/d\Omega$ scattering curves for the samples annealed at temperatures equal to or higher than 380°C with account for the appearance of a maximum at $q > q_c$, we used the relationship

$$\frac{d\Sigma(q)}{d\Omega} = \frac{A_1(D_S)}{q^n} + \frac{A_3}{((q - q_{\max})^2 + \kappa^2)^2} + I_{\text{inc}}, \quad (7)$$

where $A_3 = A_0/r_c$ is a free parameter, which is proportional to both the scattering length on nuclear density fluctuations and the density of these fluctuations; $\kappa = 1/r_c$ is the reciprocal correlation radius of nuclear density fluctuations (inhomogeneities) on which scattering occurs; and q_{\max} corresponds to the maximum position on the scattering curves. The second term in relationship (7) is squared Lorenzian and satisfactorily fits scattering on porous structures having a short-range order. In the case at hand, the short-range order in the solid phase and pores may be generated by interactions between particles of the crystal phase at early stages of their formation [14].

To arrive at ultimate results, relationship (6) and (7) were convoluted with the setup resolution function. The experimentally determined differential scattering cross section data $d\Sigma(q)/d\Omega$ were processed using least-squares fits. The fitting results are shown in Figs. 2–4 and Table 1.

These results show that D_S , the surface fractal dimension, for the xerogels precipitated at pH 6 and 9 virtually does not change as the heat-treatment tem-

Table 1. Surface fractal dimensions D_S for xerogels prepared at pH of 6, 7.5 [15], and 9 and for the products of their thermal annealing

pH	Annealing temperature, °C				
	60	270	380	500	600
6	2.18 ± 0.04	2.19 ± 0.03	2.12 ± 0.04	2.1 ± 0.04	2.01 ± 0.03
7.5	2.47 ± 0.04	2.48 ± 0.04	2.4 ± 0.05	2.29 ± 0.04	2.1 ± 0.05
9	2.62 ± 0.05	2.59 ± 0.04	2.55 ± 0.04	2.48 ± 0.04	2.4 ± 0.04

perature T_a increases from 60 to 270°C (Fig. 5). Similar results were obtained for the samples prepared by annealing $\text{ZrO}_2 \cdot x\text{H}_2\text{O}$ xerogels that had been precipitated at pH of 7.5 [15]. Thus, $\text{ZrO}_2 \cdot x\text{H}_2\text{O}$ dehydration does not induce significant alterations in the xerogel mesostructure. This is rather a nontrivial result, because metal hydroxide hydrogels usually change their structure during air drying as a result of capillary forces. In particular, Stachs and Gerber [16] mentioned that drying leads to the complete disappearance of fractal properties in gels prepared by $\text{Zr}(\text{C}_3\text{H}_7\text{O})_4$ hydrolysis.

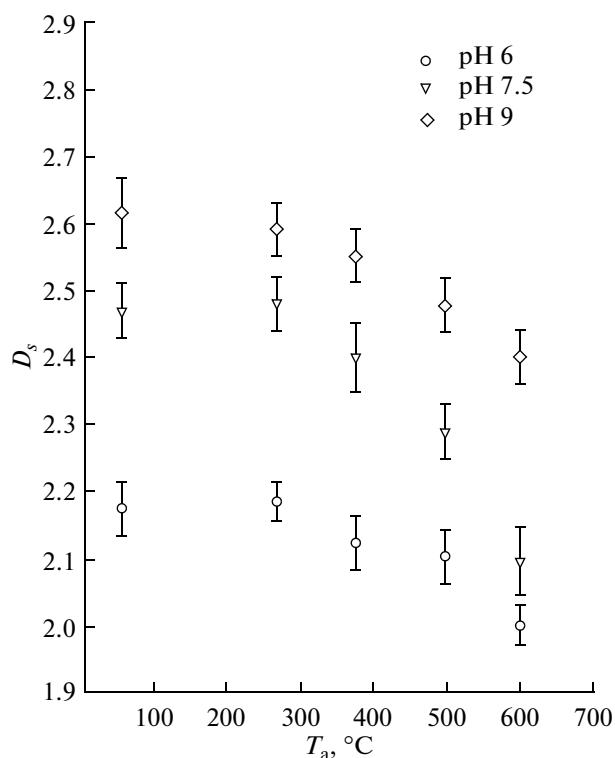
A further elevation of the annealing temperature of the xerogels prepared at pH of 6, 7.5 [15], and 9 leads to a smooth decrease in fractal dimensions. The decrease in D_S with fractal properties being maintained, in general, may be on account of surface smoothing with the maintenance of the exponential size distribution of structural elements. We observed similar trends in fractal dimension during thermal annealing for other oxide materials [17, 18]. Thus, the high-temperature annealing may be regarded as an efficient means for preparing materials with controlled surface fractal dimensions (to the value corresponding to the smooth interface, i.e., $D_S = 2$).

The mesostructure of a hydrous zirconia xerogel prepared at pH 3 and the products of its heat treatment differs considerably from the mesostructure of the samples prepared at higher pH values. As mentioned in [10], $\text{ZrO}_2 \cdot x\text{H}_2\text{O}$ gels precipitated from highly acid solutions are nonfractal ($D_S = 2$) and have very low specific surface areas ($S_{sp} < 1 \text{ m}^2/\text{g}$). Evidently, the dehydration of such gels during heating will be accompanied by structural alteration because of the appearance of a system of microcracks, which serve as channels for removal of gaseous thermolysis products. Indeed, SANS shows that the heating of a $\text{ZrO}_2 \cdot x\text{H}_2\text{O}$ sample precipitated at pH 3 produced porous samples with a so-called diffuse surface for which $n = 4 + 2\beta > 4$, where $0 \leq \beta \leq 1$ is the exponent characterizing the variation law of nuclear density ρ in the surface layer of

a particle [11]. Assuming that the particles have flat surfaces, nuclear density ρ will depend only on distance x from the surface to a point inside a particle. Thus, $\rho(x)$ for our samples may be represented as

$$\begin{aligned}\rho(x) &= 0 & x < 0 \\ \rho(x) &= \rho_0(x/\alpha)^\beta & 0 \leq x \leq \alpha \\ \rho(x) &= \rho_0 & x \geq \alpha,\end{aligned}\quad (8)$$

where α is the layer thickness within which nuclear density ρ increases from zero to ρ_0 , respectively. n and β values increase monotonically with increasing annealing temperature (Fig. 6).

**Fig. 5.** Fractal dimension D_S vs. annealing temperature for hydrous ZrO_2 samples prepared at various pH values.

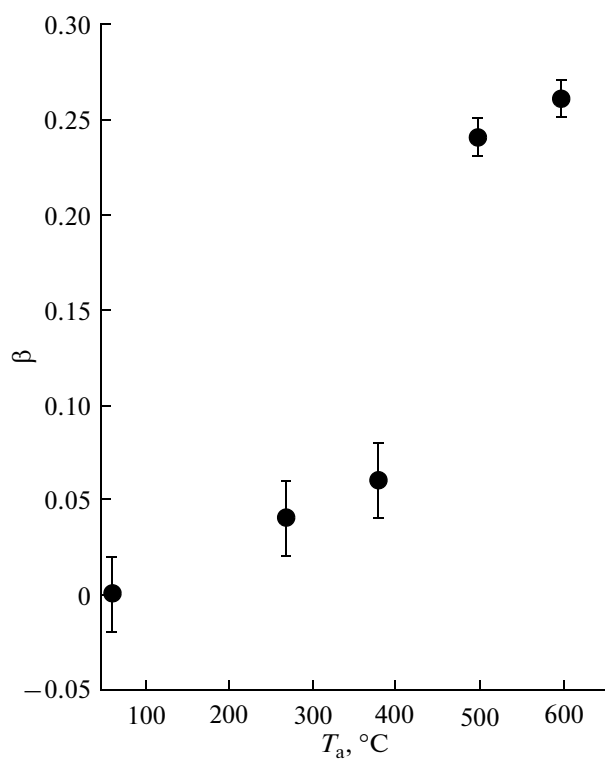


Fig. 6. Exponent β vs. annealing temperature for samples with diffuse surfaces formed during the heat treatment of the xerogel prepared at pH 3.

In turn, r_0 , the maximal size of individual particles corresponding to the lower self-similarity bound of the surface fractal, experiences more complex evolution during heat treatment (Fig. 7, Table 2). For example, the decrease in particle size observed in response to the change in annealing temperature from 60 to 270°C, is likely due to the elimination of chemically bound and sorbate water, as well as ammonium ions and nitrate ions sorbed on particle surfaces. In association, scattering in the range of $q > 0.03 \text{ \AA}^{-1}$ decreases considerably compared to the as-precipitated xerogel samples, evidently, because of the elimination of sorbate and chemically bound water during annealing. A further

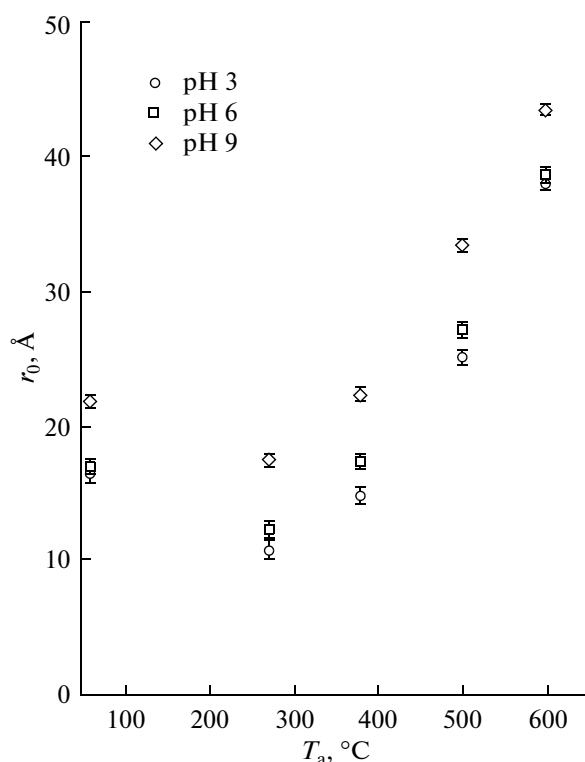


Fig. 7. Maximal size of individual particles r_0 vs. annealing temperature for hydrous ZrO_2 samples prepared at various pH values.

increase in T_a brings about a monotonic rise in r_0 associated with the coarsening of crystalline zirconia particles, which is verified by X-ray diffraction.

In summary, we have studied for the first time the mesostructure of amorphous hydrous zirconia xerogels and the products of their heat treatment. We have discovered that the heating behavior of a sample is fundamentally different depending on whether it was prepared at low or high pH. We have shown that the high-temperature annealing of hydrous zirconia xerogels prepared at various pHs is useful for manufacturing materials with controlled surface fractal dimensions.

Table 2. Maximal sizes of individual particles r_0 as determined by SANS

pH	Annealing temperature, °C				
	60	270	380	500	600
3	16.5 ± 0.7	$10.7 \pm 0.7^*$	$14.8 \pm 0.6^*$	25.0 ± 0.6	$38 \pm 0.5^*$
6	17 ± 0.7	12.3 ± 0.6	$17.3 \pm 0.5^*$	$27.1 \pm 0.5^*$	$38.7 \pm 0.5^*$
9	21.8 ± 0.5	$17.4 \pm 0.5^*$	$22.3 \pm 0.6^*$	$33.4 \pm 0.5^*$	$43.5 \pm 0.4^*$

* Values obtained with $r_0 = \pi/q_{\max}$. The other values were derived using gyration radii as $r_0 = (5/3)^{1/2} r_g$.

ACKNOWLEDGMENTS

This work was supported by the Russian Foundation for Basic Research (project nos. 09-03-12191_ofi-m and 07-02-00290-a).

REFERENCES

1. A. Harrison, *Fractals in Chemistry* (Oxford Univ. Press, Oxford, 1995).
2. W. G. Rotschild, *Fractals in Chemistry* (Wiley, New York, 1998).
3. V. K. Ivanov, N. N. Oleinikov, and Yu. D. Tret'yakov, Dokl. Akad. Nauk **386** (6), 775 (2002).
4. V. K. Ivanov, O. S. Polezhaeva, G. P. Kopitsa, et al., Neorg. Mater. **44**, 324 (2008).
5. H. Toraya, M. Yoshimura, and S. Somiya, J. Am. Ceram. Soc. **67**, C-119 (1984).
6. H. B. Stuhrmann, N. Burkhardt, G. Dietrich, et al., Nucl. Instrum. Meth. A **356**, 133 (1995).
7. D. Wignall and F. S. Bates, J. Appl. Crystallogr. **20**, 28 (1986).
8. W. Schmatz, T. Springer, J. Schelten, and K. Ibel, J. Appl. Crystallogr. **7**, 96 (1974).
9. S. Shukla and S. Seal, Int. Mater. Rev. **50**, 45 (2005).
10. G. P. Kopitsa, V. K. Ivanov, S. V. Grigoriev, et al., JETP Lett. **85**, 122 (2007).
11. P. W. Schmidt, *Modern Aspects of Small-Angle Scattering*, Ed. by H. Brumberger (Kluwer, Dordrecht, 1995), p. 30.
12. H. D. Bale and P. W. Schmidt, Phys. Rev. Lett. **38**, 596 (1984).
13. A. Guinier and G. Fournet, *Small-Angle Scattering of X-Rays* (Wiley, New York, 1955), p. 17.
14. E. Z. Valiev, S. G. Bogdanov, A. N. Pirogov, et al., Zh. Eks. Teor. Fiz. **103**, 204 (1993).
15. V. K. Ivanov, G. P. Kopitsa, S. V. Grigor'ev, et al., Fiz. Tverd. Tela. (in press).
16. O. Stachs and T. Gerber, J. Sol-Gel Sci. Technol. **15**, 23 (1999).
17. V. K. Ivanov, N. N. Oleinikov, and Yu. D. Tret'yakov, Dokl. Akad. Nauk **386**, 775 (2002).
18. V. K. Ivanov, A. N. Baranov, N. N. Oleinikov, and Yu. D. Tret'yakov, Zh. Neorg. Khim. **47** (12), 1925 (2002) [Russ. J. Inorg. Chem. **47** (12), 1769 (2002)].